The Influence of Mixed Monolayer Composition on Zinc–Carboxylate Binding at the Air–Water Interface

Research Thesis

Presented in partial fulfillment of the requirements for graduation with research distinction in Chemistry in the undergraduate College of Arts and Sciences of The Ohio State University

by Nicole Auvil

The Ohio State University April 2021

Project Advisor:

Dr. Heather C. Allen

Department of Chemistry and Biochemistry

ABSTRACT:

Sea spray aerosols (SSA) are known to have a thin organic coating that is largely comprised of fatty acids, but also contains many other organic molecules. Subphase sea water contains metal ions that have the ability to interact with this organic coating at the air-water interface, resulting in transport of metals into the atmosphere. Metal surface binding at pure monolayers has been well studied, however metal surface binding at ocean relevant mixed monolayers has not previously been studied. A model interfacial system with four monolayer ratios of stearic acid to octadecanol (100:0, 95:5, 90:10, and 85:15) is analyzed on subphases containing varying $ZnCl_2$ concentrations with a constant NaCl ionic background. Monolayers are held at a surface pressure of 35 mN/m and an approximate mean molecular area of 21.5 $Å^2$/molecule, maintaining a highly ordered film structure. Surface pressure–area (Π-A) isotherms and infrared reflection absorption spectroscopy (IRRAS) were used in conjunction to determine molecular binding interactions and quantify Zn^{2+}–carboxylate surface binding affinities at each monolayer composition. It was found that: (1) Binding affinities for all four monolayer compositions are ~300 times greater in magnitude than zinc-acetate binding in bulk aqueous solution, indicating that zinc-carboxylate binding is enhanced at the surface, and (2) Mixed monolayer composition impacts trace metal surface binding in both strength and stoichiometry.

ACKNOWLEDGEMENTS:

I would like to thank my advisor, Dr. Heather Allen, for welcoming me into her research group and always giving me insightful advice and guidance when I need it. I thank all Allen Group members, past and present, for their continuous support and for providing inspiration and direction for both my project and my life. I would like to specifically thank Maria Vazquez de Vasquez for her wonderful support and mentorship throughout the entirety of my project. Finally, I thank my parents, Chris and Susan Auvil, who taught me to apply creativity to everything I do.

Table of Contents

CHAPTER 1: MOTIVATIONS AND BACKGROUND

1.1 Atmospheric Relevance

The air-water interface is a surface that can accommodate unique chemical and physical reactions that cannot occur in the bulk. A class of molecules known as surfactants have both hydrophobic and hydrophilic characteristics and therefore tend to congregate at water's surface.[1] The air-water interface allows surfactants to orient such that the hydrophobic portion interacts with air and the hydrophilic portion interacts with bulk water, minimizing the free energy of the interfacial system.[2] Following this principle, organic molecules congregate at the ocean's surface to form a film called the sea surface microlayer (SSML). Molecules and ions are transferred from the SSML onto sea spray particles during mechanical wave action and bubble bursting, creating sea spray aerosol (SSA).[3,4] The climate is directly impacted by aerosols due to their ability to absorb and scatter solar radiation.[5] Indirect effects include aerosol particles acting as cloud condensation nuclei and ice nuclei.[6] The impact of aerosol particles on Earth's climate can be altered by organic films like the SSML.[7] Two important types of surfactant molecules naturally found in the SSML are fatty acids and fatty alcohols.[8] Their hydrophobic tails point towards the air and their hydrophilic head groups, -COOH and -OH respectively, orient towards the water.[9] Stearic Acid (SA) is a C_{18} saturated fatty acid that is known to be enriched in SSA, and octadecanol (OD) is its C_{18} saturated fatty alcohol analogue, as seen in **Figure 1**.[10,11]

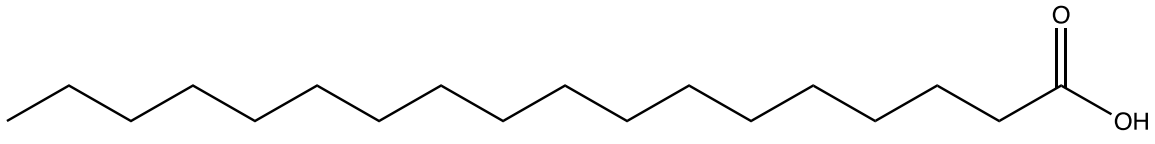

stearic acid

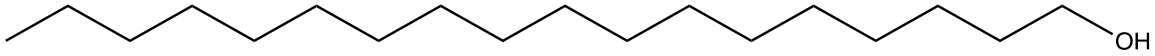

octadecanol

Figure 1. Molecular structures of stearic acid and octadecanol

SA is often used as a proxy for the organic film on SSA surfaces due to its reliable film forming behavior and atmospheric relevance.[12–14] OD is released from the breakdown of marine cell membranes and has the ability to act as an ice nucleator.[15] Fatty acid and fatty alcohol were recently discovered to exist in a nine to one ratio in oceanic emission samples.[16] An aim of this study is to emulate and observe the behavior of a mixed monolayer at this ocean relevant ratio.

1.2 Subphase Metal Ion Impacts on Interfacial Molecules

Ions in the bulk water are known to interact with organic surface films, altering the orientation and packing of surfactant molecules.[17–19] This interaction occurs due to the polarity of surfactant head groups. Previous studies have shown considerable surface ordering effects when divalent cations such as Zn^{2+} interact with a SA monolayer, indicating strong binding and even metal-induced deprotonation of the -COOH group.[18,20,21] Monovalent Na^{+}, on the other hand, does not interact as strongly with SA's carboxylate head group due to its smaller charge and larger ionic

radius.[18,19] When compared to the strength of SA, OD is assumed to be neutral and nonbinding due to its hydroxy headgroup, which has been found to exhibit insignificant metal binding.[18]

Major ionic metal components of seawater like Na^+ and Ca^{2+} have been detected in SSA.[22] Trace metal ions such as Zn^{2+} and Fe^{3+} have oceanic concentrations several orders of magnitude lower than major metal ionic components, yet have been found to be enriched in SSA at significantly higher relative proportions.[23,24] Ion-surfactant interactions are the reason for this disparity in SSA enrichment. Na^+ can only partake in weaker ionic interactions with surfactant headgroups.[25] Trace metals, however, typically have the ability to form strong covalent bonds with surfactant headgroups and have therefore been found in the SSML at concentrations reaching one hundred times above those found in the subsurface bulk seawater.[18,26] When wave breaking or bubble bursting events occur, trace metals are transferred into SSA along with the surfactants to which they are bound.

Zn^{2+} is a biological micronutrient required by marine organisms to survive.[27] It is known to have an average oceanic concentration of 6 nM and a very high SSML enrichment factor relative to other oceanic metal ions despite its low concentration.[18,24] For scale, the total concentration of multivalent trace metals in the ocean is estimated to be about 164 nM.[24] Zn^{2+} was chosen as the model trace metal in this study due to its strength in interaction with a monolayer of SA.[18] Na^+ is the most concentrated metal ion in the ocean, with an average concentration of 468 mM.[24] It was chosen to create a constant, ocean relevant ionic background that would not inhibit the surface interactions of Zn^{2+}.

1.3 Principles and Challenges of a Mixed Monolayer

A pure monolayer is heterogeneously composed of only one type of surfactant, whereas a mixed monolayer contains a combination of two or more surfactants at the air-water interface[28]. Due to the immense diversity in sources from which atmospheric and oceanic organics originate, mixed monolayer films are more suitable than pure monolayers for the purpose of representing SSA and the SSML. Experimental techniques and molecular dynamics computations have both been used to study the interfacial properties of mixed monolayers at the air-water interface.[12,29,30] Specifically, the surface properties of binary mixtures of fatty acids with other organics such as amines, esters, cholesterols, and alcohols have been well studied during the past two decades.[29,31,32] These studies have revealed substantial differences between the physical and chemical properties of a pure fatty acid monolayer and a mixed monolayer that contains fatty acid. The inclusion of a secondary surfactant in a fatty acid monolayer has been shown to alter film packing structure[12], thermodynamic behavior[32], and monolayer stability[29].

While the complexity of mixed monolayers allows for better representation of real-world systems, it also creates experimental challenges. One issue is the physical creation of a mixed monolayer. Surfactant molecules have a certain amount of immiscibility with each other and can create domains on water's surface instead of mixing to form an ideal homogenous film.[28] In 2015, Lee et al. conducted a study to determine the best method for creating a homogenously mixed multi-component monolayer that contains SA and other surfactants.[33] They found that the main factor in monolayer mixing is the spreading method used in preparing the monolayer. When SA and the other surfactant are prepared in separate solutions and spread individually onto the subphase water, the two surfactants cannot mix well, resulting in distinct domain formation.[33] However, when SA and the other surfactant are pre-mixed in the spreading solvent prior to

spreading on the subphase, a well-mixed monolayer is formed.[33] Another inconvenience of mixed monolayers lies within the complexity of data deconvolution. Ge et al. noted in their 2013 study that the molecular properties for each component in a mixed monolayer are difficult to individually analyze using spectroscopic techniques.[34] Due to this challenge, lateral interactions between surfactant molecules in a mixed monolayer are not well understood.

1.4 Objectives

Monolayer composition has the ability to affect structure and stability of lipid films at the air-water interface. However, no previous studies have investigated how monolayer composition impacts trace metal surface enrichment. The numerous studies that currently exist in the realm of metal surface binding observe only a single-component monolayer[17–19]. The primary goal of this study is to probe the effect of mixed monolayer composition on trace metal surface binding. Mixed monolayers composed of SA and OD are systematically studied at four different ratios, and each ratio is studied on eight subphase concentrations of $ZnCl_2$ with a constant NaCl ionic background. Infrared reflection–absorption spectroscopy (IRRAS) is used to probe the monolayer packing of mixed surface films and quantify apparent surface binding constants using the methylene scissoring band and the carboxylate asymmetric stretch, respectively.

CHAPTER 2: AIR–WATER INTERFACE AND TRACE METAL BINDING

2.1 Pure Monolayer Metal–Carboxylate Surface Binding

Fatty acid monolayers at the air-water interface of ion-containing subphases have received considerable attention in previous studies.[18,20,25,35,36] SA monolayers are known to have protonated carboxylic headgroups while on a pure water subphase (**Figure 2a**), but when the subphase contains ions the headgroups become deprotonated into carboxylate groups due to a reduction in the surface pKa as a result of ion affinity for the negatively charged headgroups (**Figure 2b**).[36,37] When the subphase ion is Zn^{2+}, very strong metal ion-carboxylate interactions are known to occur.[18] These interactions take the form of covalent, contact ion pairing with an unsymmetric bidentate chelating configuration.[35,36] Bidentate chelation structure is shown in **Figure 2c**.

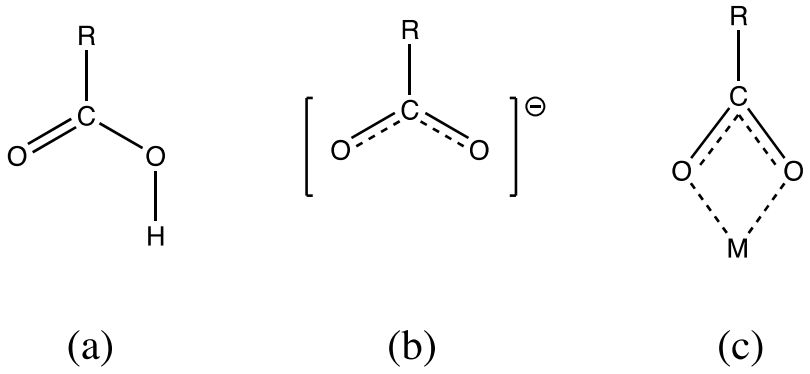

Figure 2. (a) Protonated carboxylic group on a subphase of pure water. (b) Ion-containing subphase, resulting in headgroup deprotonation and the formation of a carboxylate group. (c) Bidentate chelating bond, both oxygen atoms bond to the metal cation.[38]

Metal-carboxylate surface interactions may also have an impact on lateral interactions between carboxylate headgroups. On a pure water subphase, SA monolayers form a hexagonal subcell structure. This structure changes when the subphase contains certain metal ions, but for

Zn^{2+} the lateral interactions maintain a hexagonal structure.[36] Another aspect of monolayer structure that may be changed due to metal surface binding is the tilt of the surfactant hydrocarbon chains. On pure water, SA hydrocarbon chains have a 20° tilt angle relative to the surface normal. When the subphase contains Zn^{2+}, however, the SA molecules are thought to orient completely vertically (0° tilt angle).[36]

2.2 Mixed Monolayer Metal–Carboxylate Surface Binding

Zn^{2+} certainly has strong interactions with a monolayer composed of pure SA. However, it is unknown how these interactions may be altered by the addition of a secondary surfactant. Fatty acids and fatty alcohols are miscible within a monolayer, indicating that their headgroups may interact laterally[16]. It follows that fatty alcohol molecules have the potential to disrupt lateral interactions between the fatty acid molecules, potentially altering their ability to adsorb trace metals. If a SA monolayer is diluted with a certain amount of OD, then lateral carboxylate headgroup interactions as well as metal-carboxylate interactions may be impacted.

A major concern about mixed monolayer studies is that contributions from individual surfactant types are difficult to differentiate in the collected data. In this study, SA binding interactions are able to be isolated due to the non-binding nature of OD and the distinct carboxylate region in the IRRAS spectrum, 1360-1900 cm^{-1}. Therefore, all binding reported in this study is due solely to Zn^{2+}–carboxylate surface interactions, which may be altered due to the inclusion of OD in the monolayer.

2.3 Langmuir Monolayers and Surface Pressure – Area Isotherms

Langmuir monolayers are monomolecular films of a given surfactant at the air-water interface.[39] Typically, the surfactants within Langmuir monolayers are structurally composed of hydrophilic headgroups with at least one long, hydrophobic alkyl chain. In order to create a monolayer experimentally, the surfactant is dissolved in a volatile organic solvent and deposited dropwise on water's surface with a syringe. The solvent evaporates, leaving a monolayer film in which hydrophilic headgroups interact with water molecules at the surface, while the hydrophobic surfactant tails point away from the water. The amount of surfactant present at the surface of a spread monolayer is assumed to be the total amount in the system.[28] Langmuir monolayers are useful for interfacial binding studies because they maintain a fundamental level of physical simplicity while offering precise control over area per surfactant molecule.[39] Due to these attractive qualities, Langmuir monolayers have widely been used to emulate oceanic and atmospheric membranes like the SSML.[36]

Surface pressure–area (Π-A) isotherms are a method of analysis often used in the investigation of Langmuir monolayers at the air-water interface. Surface pressure is measured as a function of the area of the water's surface available to each surfactant molecule (mean molecular area).[9] In order to accomplish this measurement, the subphase is placed in a Teflon trough and a monolayer is spread on the surface. After the organic solvent evaporates, Teflon barriers are swept across the surface at a specific rate, decreasing the total surface area and mean molecular area. The mean molecular area is mathematically determined from the known area of the trough, the known distance the barriers have moved, and the known number of surfactant molecules on the surface.[9] The surface pressure is monitored using a Wilhelmy plate attached to a Langmuir film balance. The plate hangs from the balance, partially submerged in the water. It measures surface tension,

which can be mathematically converted to surface pressure given the area and thickness of the plate.[9]

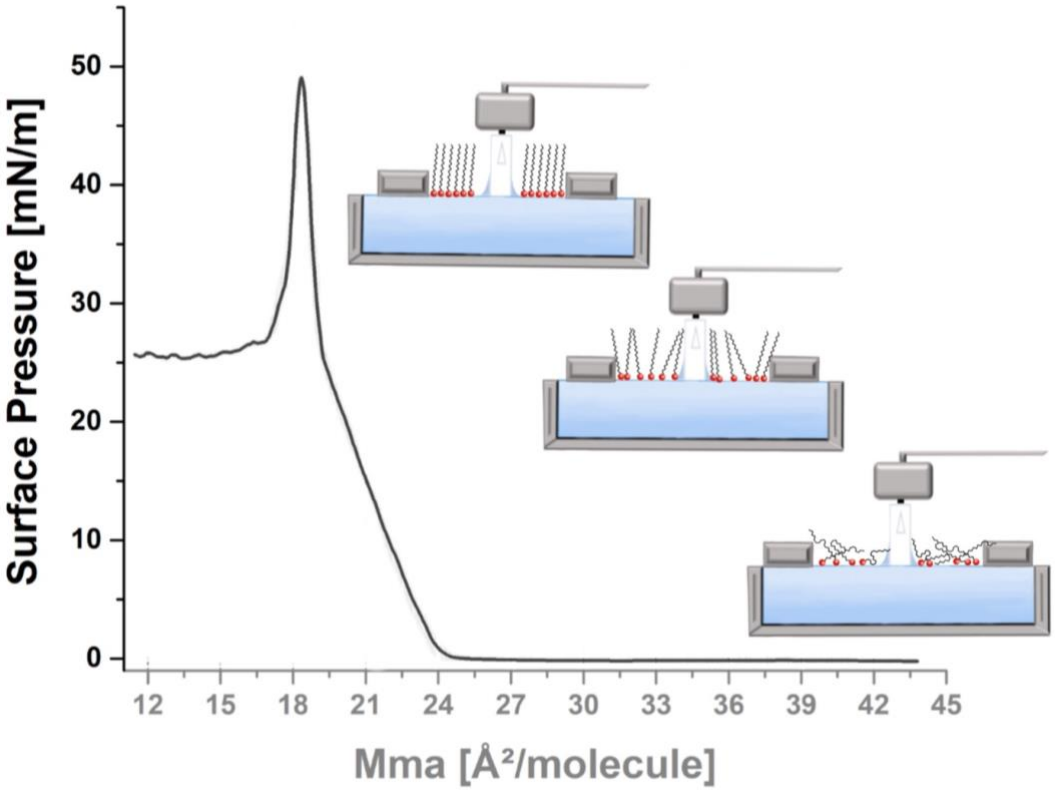

Figure 3. Example output of a Langmuir Π-A isotherm, showing schematic orientation of the pure surfactant monolayer as the barriers compress and mean molecular area is reduced. To be read from right to left[9]

The measurements of surface pressure and mean molecular area collected during barrier compression are typically displayed in a plot of surface pressure vs mean molecular area (**Figure 3**). This plot, known as an isotherm, contains distinct discontinuities that define the phases of the isotherm. The phase behavior is determined by the chemical and physical properties of the surfactant, the subphase contents, and the subphase temperature.[9] Upon spreading, the monolayer exists in the gas-liquid expanded coexistence phase. This state is characterized by loose molecular packing, low surface pressure, and low degree of organization of hydrophobic tails. After

compression of the monolayer, the molecules move closer to each other and become more ordered, with hydrocarbon tails losing their gauche defects to adopt a more trans conformation.[40] This is known as the tilted condensed phase. With further compression the monolayer reaches the untilted condensed state in which the hydrophobic tails are highly ordered and packed closely together.

Meaningful information can be extracted from Π-A isotherms. An isotherm may be more condensed than expected due to attractive forces between surfactant molecules or more expanded than expected due to repulsive forces between surfactant molecules.[9] These attractive and repulsive forces can be influenced by the components within the subphase. For example, a monolayer of SA on a subphase of $ZnCl_2$ produces an isotherm that occurs at a more condensed mean molecular area than that on pure water.[36] The $ZnCl_2$ isotherm also contains less apparent phase transitions than the water isotherm. Particularly, Zn^{2+} removes the tilted-condensed phase. This indicates that when Zn^{2+} binds to the headgroup of SA, the monolayer remains untitled and therefore as tightly packed as possible in its condensed phase. Surface pressure-area isotherms provide useful insight into the binding and packing interactions of a Langmuir monolayer, but do not reveal detailed microscopic information.[36]

2.4 Infrared Reflection Absorption Spectroscopy

IRRAS is one of the leading methods for analysis of Langmuir monolayers. It provides information that allows for the characterization of chain conformations, the identification of functional groups at the surface, and the determination of surface binding affinities.[36,41] An IRRAS setup typically involves an infrared beam reflected from a mirror and focused on a Langmuir monolayer at the air-water interface. When the beam hits the monolayer, the infrared light perturbs surfactant molecular vibrations, creating an oscillating dipole moment which is characteristic of

bond vibrations between certain atoms.[42] The beam that now contains this molecular information is reflected from the surface to another mirror and finally into the detector.[43]

IRRAS data is presented as reflectance-absorbance (RA) versus wavenumber, where RA is defined by **Equation 1** below.

$$RA = -log_{10}\left(\frac{R}{R_0}\right) \quad (1)$$

Where R_0 is the reflectance of the bare subphase, and R is the reflectance of the Langmuir monolayer on top of the subphase. The analysis of RA data is based on spectral band frequency and intensity. Hydrocarbon chain conformation of the surfactants in the monolayer can be determined by looking at the CH_2 symmetric and asymmetric stretching vibrational bands.[42] Additionally, the vibrational modes of the surfactant molecules' headgroups provide information about subphase-surfactant binding interactions.[18,36,41] Surface binding affinities can be quantified via IRRAS using the techniques presented by Neal et al. in their study of molecular enrichment at the monolayer.[41]

Fatty acid monolayers have been extensively studied using IRRAS, resulting in well-defined characteristic frequencies of carboxylate and hydrocarbon chain vibrations.[18,20,25,35,36] Modes of interest within the carboxylate region include the carbonyl (C=O) stretch at ~1750–1700 cm^{-1}, the carboxylate (COO^-) asymmetric stretch at ~1530–1550 cm^{-1}, and the carboxylate (COO^-) symmetric stretch at ~1400 cm^{-1}.[20,36] When the subphase contains ions, the carbonyl stretch disappears and the carboxylate stretches grow in due to deprotonation of the functional group. This region of the spectrum shows that Zn^{2+} binds to the carboxylate headgroup of SA to form an unsymmetric chelating bidentate complex, shown in **Figure 2c**.[20] Additionally, the position of the alkyl (CH_2) symmetric and asymmetric bands are known to be sensitive to the orientation of hydrocarbon tail chains. Lower wavenumbers are characteristic of highly ordered all trans

conformers, while the number of gauche defects increases with the wavenumbers of the modes, typically known as a blue shift.[20]

IRRAS provides information about all molecules at and near the air-water interface. This technique is sensitive enough to effectively probe surface monolayers, but it is not truly surface-specific because its probing depth is a few μm.[44] Due to this range of analysis depth, humidity above the monolayer surface can be an issue, especially in the carboxylate region.[43] This type of interfacial water vapor, when probed by IRRAS, creates a considerable amount of noise in the range of 1360-1900 cm^{-1}, which is the region of interest in this study.

CHAPTER 3: MATERIALS AND METHODS

3.1 Materials and Sample Preparation

The materials used in this study were purchased commercially and used without further purification unless otherwise noted. Stearic acid (C_{18} fatty acid, Sigma-Aldrich, ≥ 98.5% grade 1) and octadecanol (C_{18} fatty alcohol, 99%, Sigma-Aldrich) were dissolved in chloroform (HPLC Grade, Fisher Scientific) to create ~3.8 mM stearic acid and stearyl alcohol stock solutions. These solutions were combined in varying proportions to prepare ~3.8 mM mixed solutions at the ratios 100:0, 95:5, 90:0, and 85:15 SA:OD (w/w). Sodium chloride salt (NaCl) (99.999% trace metals basis, Aldrich, and 99.998% trace metals basis, Fisher Scientific) was baked in a furnace at 675°C for >8 hours to remove possible organic contamination. Zinc chloride salt ($ZnCl_2$) (99.999% trace metals basis, Aldrich) was used as is. NaCl and $ZnCl_2$ salt solutions were prepared used ultrapure water with a resistivity of 18.2 MΩ•cm (Milli-Q® Advantage A10, MilliporeSigma, Burlington, MA). The NaCl solution was filtered through Dionex OnGuard II M cartridges (Thermo Fisher Scientific) to remove possible trace metal impurities. NaCl and $ZnCl_2$ solutions are combined in the Langmuir trough to create the subphase. The measured pH for the highest and lowest concentrations of mixed salt solutions are 5.8 and 5.5, respectively, and these pH values are the maximum deviations from pure water.

3.2 Methods

3.2.1 Surface Pressure – Area Isotherms

While Π-A isotherms were not directly used in the determination of zinc–carboxylate surface binding constants, they were necessary for maintaining monolayer surface pressure during IRRAS scans and calibrating surfactant solution concentrations. Π-A isotherms were performed on a Teflon Langmuir trough with an area of 144.5 cm^2 fitted with movable Delrin barriers (KSV NIMA, Finland). Surface pressure was measured using custom cut filter paper Wilhelmy plates (ashless grade, Whatman). The trough and barriers were rigorously cleaned with reagent alcohol and ultrapure water and dried before each trial. After the aqueous subphase solution is added to the trough, its surface is checked for contamination by compressing the barriers and ensuring that the surface pressure does not rise above 0.2 mN/m. The surfactant solutions were deposited onto the surface dropwise with a microsyringe (Hamilton) in order to create the monolayer. The syringe was cleaned thoroughly between each trial with reagent alcohol, set to dry, and then rinsed ten times with chloroform (HPLC Grade, Fisher Scientific). The system was then left idle for ten minutes to allow for chloroform evaporation. The resulting monolayer was compressed at a constant rate of 5 mm/min per barrier until a surface pressure of 35 mN/m was achieved. In order to maintain this surface pressure, the barriers then moved back and forth synchronously at a slow rate of 1 mm/min. All isotherms were repeated three times to ensure repeatability. The concentrations of the stearic acid and stearyl alcohol stock solutions were calibrated to 24 and 21 $Å^2$/molecule, respectively.[45] All trials were run at 21 ± 1 °C and at a relative humidity of 31 ± 9%.

Figure 4. Experimental setup featuring Langmuir trough, barriers, Wilhelmy plate, FTIR spectrometer, and mirrors

3.2.2 Infrared Reflection Absorption Spectroscopy

IRRAS was the primary technique used to analyze Zn^{2+}–carboxylate binding. All IRRAS spectra were collected with a Fourier transform infrared (FTIR) spectrometer (Frontier, Perkin Elmer) equipped with an HgCdTe (MCT) detector that is cooled with liquid nitrogen. Within the spectrometer, the Langmuir trough sits on a breadboard alongside two planar gold-plated mirrors positioned such that the beam reflects off of the monolayer at an incident angle of 48° relative to surface normal (**Figure 4**). The incident unpolarized IR beam is reflected off the input gold mirror and onto the surface, where the beam interacts with the interface and is then reflected to the output

mirror and finally to the detector. IRRAS scans were taken at 35 mN/m, a surface pressure at which the monolayer is in condensed phase. All spectra were collected immediately after the surface pressure hit 35 mN/m. Spectra are plotted as reflectance-absorbance (RA), calculated using **Equation 1,** versus frequency. Each spectrum is an average of 400 scans in single beam mode with a resolution of 4 cm^{-1}. Baseline correction by a 4^{th} order polynomial in the region of interest and other data processing were completed using the program OriginPro 9 (OriginLab 9, Northampton, MA). All spectra shown here are averaged from at least three spectra using OriginPro 9's average function. The reported uncertainties are considerable due to spectral noise from water vapor. Reported binding affinity standard errors encapsulate uncertainty from spectral uncertainty as well as fitting uncertainty.

3.2.3 Experimental Setup

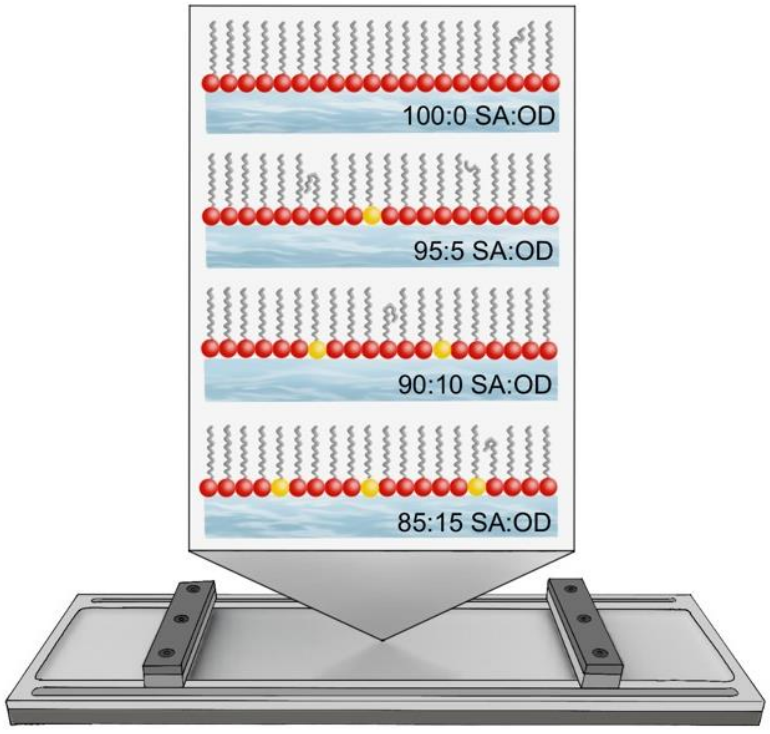

Figure 5. A schematic of the mixed monolayer ratios used in this study. The molecules with red headgroups represent SA; the yellow is OD. Hydrocarbon chains have an almost all-trans conformation. A Langmuir trough is depicted as the vessel.

In order to determine the influence of monolayer composition on trace metal surface binding, surfactant headgroup-ion interactions were probed using surface-sensitive IRRAS in conjunction with Π-A isotherms. The SA:OD monolayer ratios examined were 100:0, 95:5, 90:10, and 85:15 (**Figure 5**). Each monolayer ratio was analyzed over aqueous subphase solutions consisting of a constant NaCl ionic background (468 mM) with eight varying $ZnCl_2$ concentrations (0-25 mM). The NaCl ionic background has an ionic strength of 468 mM and when the highest concentration of $ZnCl_2$ is included, the ionic strength of the subphase increases to 543 mM. While the largest difference in subphase molarity across all measurements is 25 mM, the difference in ionic strength is 75 mM due to the charge of the zinc ion. The molecular interaction of interest is the binding of the divalent metal cation, Zn^{2+}, to the carboxylate headgroups within the monolayer. The intensity of the asymmetric carboxylate band at each concentration is normalized and fit to an adsorption curve in order to calculate the surface binding constant of Zn^{2+} at each ratio of fatty acid to fatty alcohol. This allows for quantitative comparison of binding between the monolayer compositions.

CHAPTER 4: RESULTS AND DISCUSSION

4.1 Zinc–Carboxylate Surface Interactions

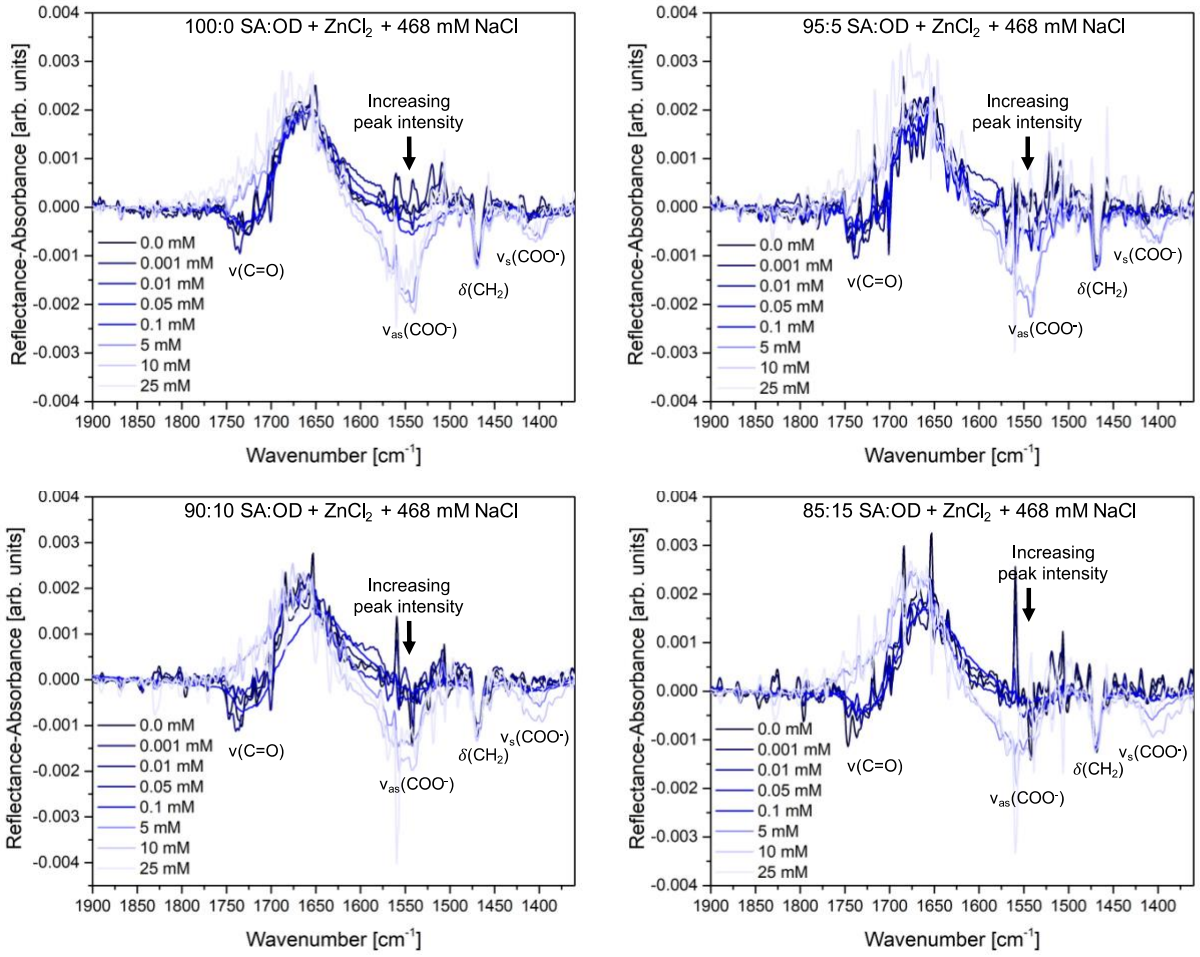

Figure 6. Carboxylate region of IRRAS spectra of SA:OD mixed monolayers in the ratios 100:0 (top left), 95:5 (top right), 90:10 (bottom left), and 85:15 (bottom right). All scans have a subphase containing 468 mM NaCl, a variable amount of $ZnCl_2$, and a surface pressure of 35 mN/m.

IRRAS spectra of the four different monolayer compositions on a range of $ZnCl_2$ subphase concentrations were utilized to study Zn^{2+}-carboxylate surface binding at the air-water interface (**Figure 6**). All presented spectra have had the subphase background spectrum subtracted and

therefore contain information specific to the monolayer film. As previously discussed, this region of an IR spectrum is susceptible to considerable noise due to water vapor occurrence near the surface of the subphase. Most notably, the sharp and narrow peak at 1558 cm^{-1} in all four ratios is an artifact of water vapor noise. Despite this inconvenience, the signal to noise in these spectra is strong enough to provide meaningful information. The location of the methylene scissoring band $\delta(CH_2)$ at 1469 cm^{-1} confirms that the hydrocarbon chains are packed in a hexagonal subcell structure.[46] The spectra also reveal the carbonyl stretch $\nu(C=O)$ at 1729 cm^{-1}, the carboxylate symmetric stretch $\nu_s(COO^-)$ at 1404 cm^{-1}, and the carboxylate asymmetric stretch $\nu_{as}(COO^-)$ at 1546 cm^{-1}. These values are all consistent with previous studies.[20,36] It is seen across all monolayer compositions that the $\nu_{as}(COO^-)$ mode increases in area and intensity with increasing Zn^{2+} concentration. This pattern is indicative of binding interaction between Zn^{2+} and the carboxylate headgroup of SA. In addition, the disappearance of the $\nu(C=O)$ mode with increasing Zn^{2+} concentration indicates that the Zn^{2+}–carboxylate binding interaction is primarily unsymmetrical bidentate chelation, although contributions due to other binding geometries are also possible. Since the carboxylate stretching mode has shown sensitivity to binding, it can potentially act as a probe of zinc–SA binding interactions across monolayer compositions.[20,35,36,41]

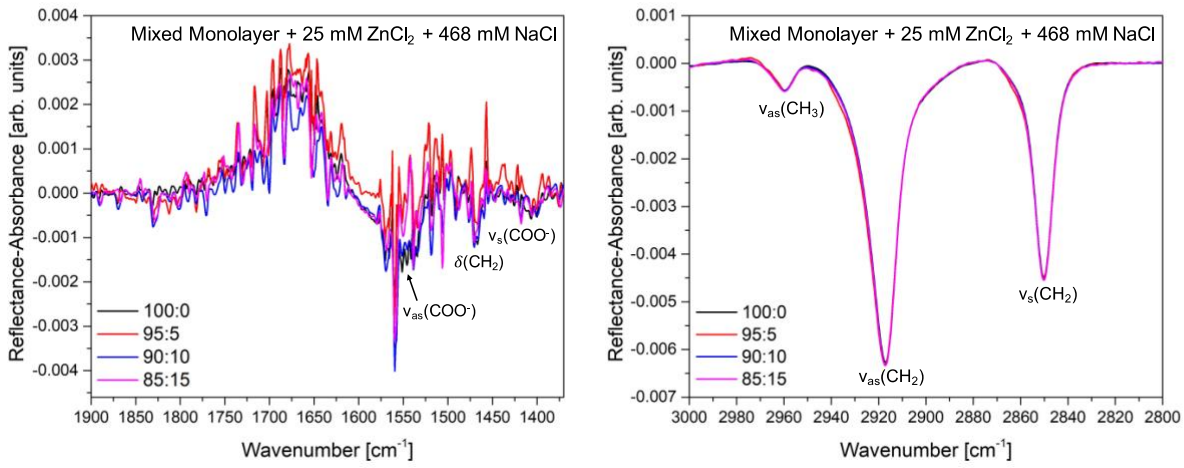

Figure 7. Carboxylate (left) and alkyl (right) regions of IRRAS spectra of each monolayer composition on a subphase of 25 mM $ZnCl_2$ and 468 mM NaCl at a surface pressure of 35 mN/m.

The spectra of all four monolayer compositions on the most concentrated $ZnCl_2$ subphase are compared in **Figure 7**. The ν(C=O) mode at 1729 cm^{-1} is nonexistent at this concentration, indicating full deprotonation of the carboxylate headgroups as well as Zn^{2+}–carboxylate chelation. Most notably, the area of the $\nu_{as}(COO^-)$ peak varies among monolayer compositions on the same subphase. In the alkyl region, the methylene asymmetric stretch $\nu_{as}(CH_2)$ is found at 2918 cm^{-1} and the methylene symmetric stretch $\nu_s(CH_2)$ is found at 2851 cm^{-1}. Though they are not shown in a figure, these modes are located at the same wavenumbers for all concentrations of zinc. The positions of these two modes indicate that the monolayer's hydrocarbon tails take an almost all-trans conformation.[36]

Furthermore, the $\nu_{as}(COO^-)$ peak areas for all subphase $ZnCl_2$ concentrations are displayed **Figure 8**. At low $ZnCl_2$ concentrations, it is observed that peak areas do not vary significantly between monolayer compositions. However, they do at higher $ZnCl_2$ concentrations. Since the $\nu_{as}(COO^-)$ mode is sensitive to binding interactions, this variation may suggest that the inclusion of OD in a monolayer of SA can impact the ability of SA molecules to bind Zn^{2+}.

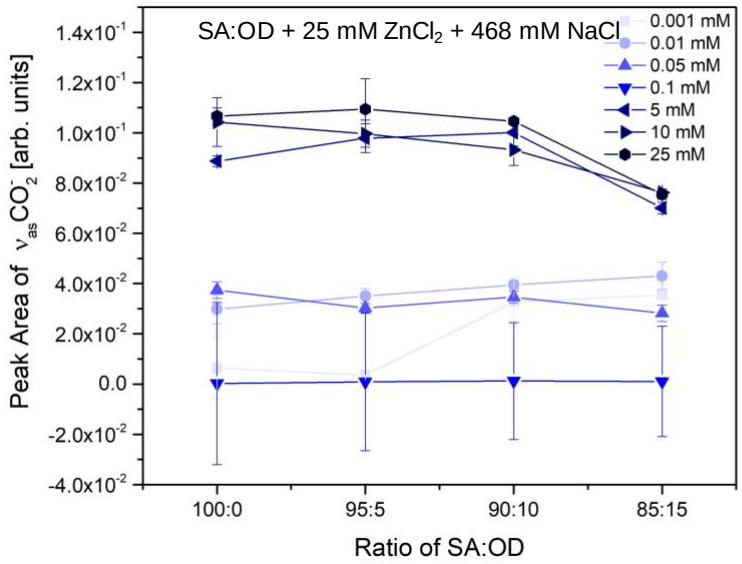

Figure 8. Integrated peak area of the $\nu_{as}(COO^-)$ mode displayed for each subphase $ZnCl_2$ concentration across all monolayer compositions. Error bars indicate one standard deviation.

All monolayers in this study were compressed and held at a surface pressure of 35 mN/m with an approximate mean molecular area of 21.5 $Å^2$/molecule while IRRAS scans were taken. At this surface pressure, a monolayer of SA on a zinc-containing subphase exists in the highly ordered untitled condensed phase.[36] While this system is not at equilibrium, the highly ordered metastable state may be more representative of atmospheric and ocean films in nature. Dynamic wave oscillation at the ocean's surface and the shrinking of SSA particles in the atmosphere due to evaporation can cause surface films to expand and condense, resulting in deviation from the equilibrium state. Because these film perturbations are ubiquitous in moving water, a non-equilibrium system is suitable for their emulation. Additionally, fatty acid molecules such as SA have been found to form complex three-dimensional aggregates at the air-water interface under certain conditions, disrupting the two-dimensional monolayer structure.[47] The high surface

pressure and subphase ionic strength used in this study may play a role in inhibiting the formation of these aggregates, thus stabilizing the monolayer throughout measurement.[48]

4.2 Determining Surface Binding Affinity

4.2.1 Adsorption Curves and Fitting

Table 1. Normalized carboxylate asymmetric peak areas with standard error for each zinc concentration and monolayer composition.

	Normalized $\nu_{AS}(COO^-)$ Peak Area			
Zn^{2+} Concentration (mM)	100:0	95:5	90:10	85:15
0	0	0	0	0
0.001	-0.072 ± 0.143	-0.063 ± 0.039	0.118 ± 0.127	0.321 ± 0.074
0.01	0.179 ± 0.085	0.253 ± 0.058	0.201 ± 0.054	0.449 ± 0.093
0.05	0.260 ± 0.069	0.205 ± 0.049	0.141 ± 0.056	0.198 ± 0.059
0.1	0.205 ± 0.063	0.176 ± 0.050	0.002 ± 0.063	0.093 ± 0.033
5	0.808 ± 0.081	0.884 ± 0.132	0.945 ± 0.093	0.907 ± 0.052
10	0.974 ± 0.134	0.902 ± 0.132	0.860 ± 0.099	1.012 ± 0.044
25	1 ± 0.094	1 ± 0.179	1 ± 0.069	1 ± 0.051

To quantify the binding ability of SA in each monolayer composition, binding affinities were determined based on asymmetric carboxylate stretch peak area. The peak areas, shown in **Table 1**, were quantified via peak integration and normalized via min-max normalization, meaning that a value of 0 corresponds to the peak area on a subphase of 0 mM $ZnCl_2$ and 468 mM NaCl and a value of 1 corresponds to the peak area on a subphase of 25 mM $ZnCl_2$, 468 mM NaCl. Since the minimum value is normalized to the peak area of a system containing only the background NaCl and no $ZnCl_2$, the binding indicated by these peak areas is assumed to be solely due to zinc–SA interactions. The reported error values are standard error, and they were propagated through the addition, subtraction, and division used in normalization.

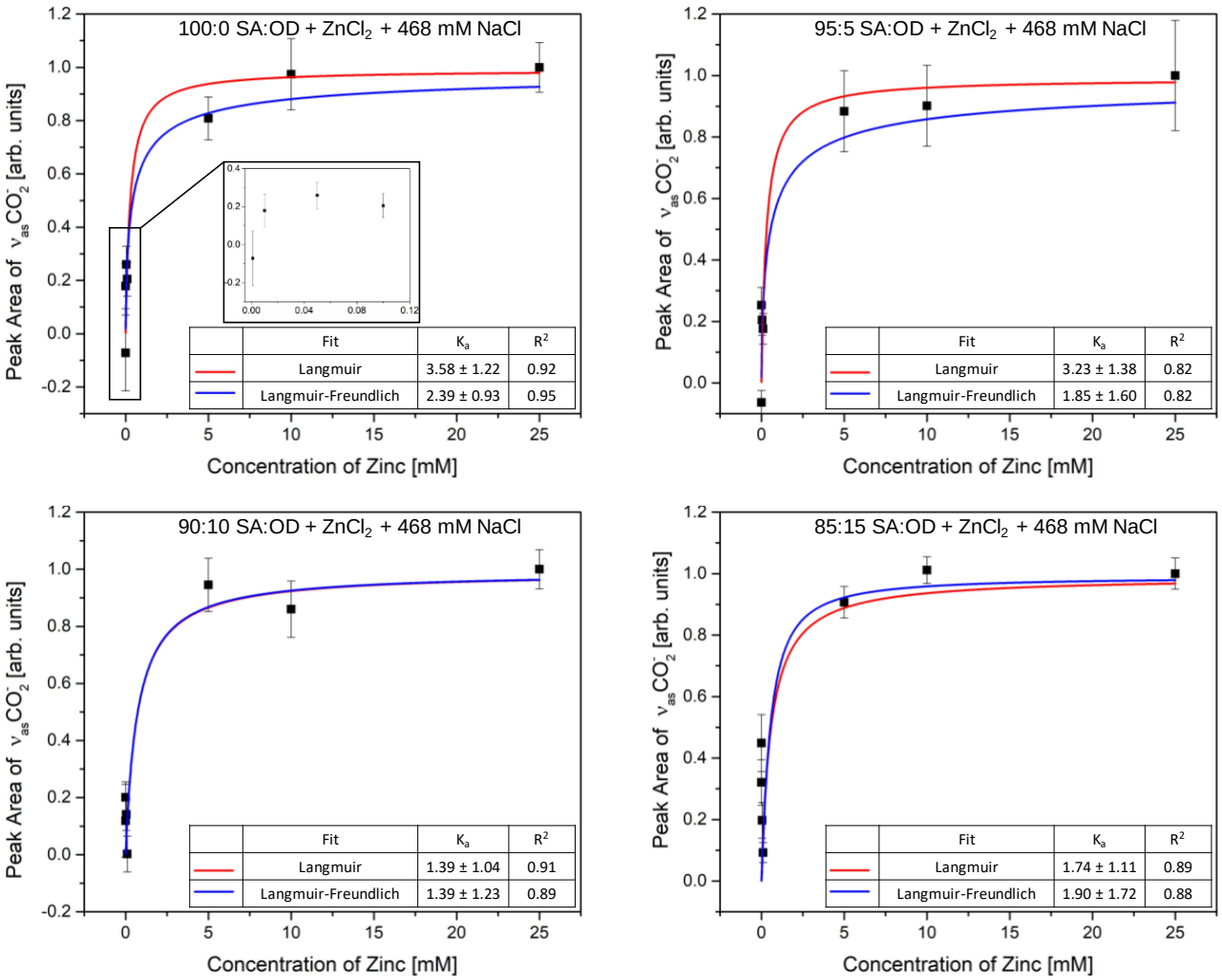

Figure 9. The normalized peak area of $\nu_{as}(COO^-)$ of SA:OD mixed monolayers in the ratios 100:0 (top left) with inset showing low concentration regime, 95:5 (top right), 90:10 (bottom left), and 85:15 (bottom right). All scans have a subphase containing 468 mM NaCl, a variable amount of $ZnCl_2$, and a surface pressure of 35 mN/m. Surface binding affinities found by each adsorption model are given as mM^{-1}.

Results were plotted as concentration of zinc versus normalized peak area of $\nu_{as}(COO^-)$, separated by monolayer composition. The plots were fit to two different surface adsorption models, Langmuir and Langmuir Freundlich (**Equations 2, 3**)

$$\text{Langmuir} \qquad A = A_{max}\frac{K_a[Zn^{2+}]}{K_a[Zn^{2+}]+1} \tag{2}$$

$$\text{Langmuir-Freundlich} \qquad A = A_{max}\frac{[K_a[Zn^{2+}]]^n}{[K_a[Zn^{2+}]]^n+1} \tag{3}$$

where A and A_{max} are peak intensity and maximum peak intensity of $\nu_{as}(COO^-)$, $[Zn^{2+}]$ is the bulk concentration of zinc, n is a physical constant, and K_a is the affinity constant for adsorption.[41,49–51] For both adsorption models, the binding was assumed to have occurred at a 1:1 ratio of zinc to SA. The Langmuir adsorption model is a popular method for quantifying how an adsorbate forms a layer on a given surface based on the equilibrium of ions between the two phases.[52–54] Because the simplifications are severe in this model, modifications have been developed to create more realistic models.[51] The Langmuir-Freundlich adsorption model is one such equation. It includes an exponential term and a physical constant that introduce the possibility of adsorption occurring in multiple layers.[51,54] This feature can be useful for analyzing adsorption on non-uniform surfaces, such as a mixed monolayer.

The normalized plots with propagated error and modeled adsorption curves are given in **Figure 9**. All four monolayer compositions show an increase in peak area with zinc addition. Based on R^2 value, the Langmuir-Freundlich model provides the best fit for 100:0, while the Langmuir model provides the best fit for 90:10 and 85:15. The two adsorption models provide an equally good fit for 85:15. Across all monolayer compositions, differences in quality of fit between the two models are minimal.

4.2.2 Binding Affinity Quantification

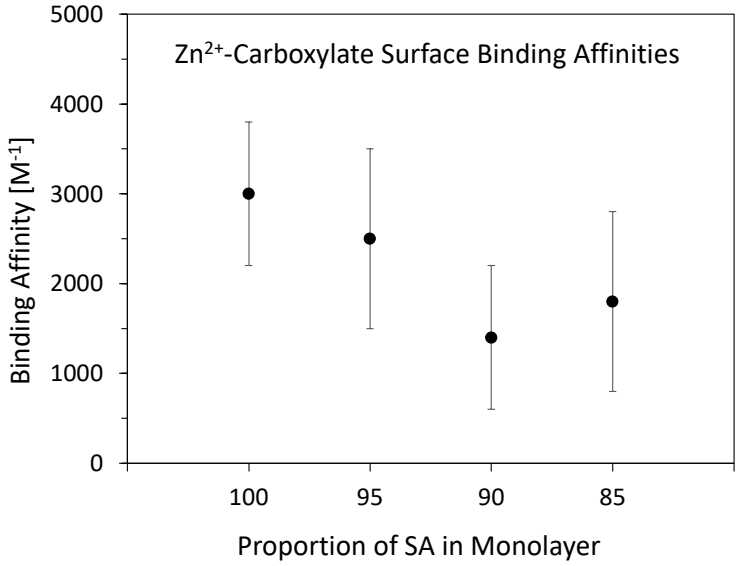

SA:OD Ratio	Binding Affinity (M^{-1})
100:0	3.0 (0.8) × 10^3
95:5	2.5 (1.0) × 10^3
90:10	1.4 (0.8) × 10^3
85:15	1.8 (1.0) × 10^3

Figure 10. Summary of the binding affinities of carboxylate to Zn^{2+} for each of the four reported monolayer compositions with standard error

Zinc–carboxylate surface binding affinities found for each monolayer composition by both adsorption models are given in **Figure 9**. The reported error is standard error, propagated through the average. Since both adsorption models provide statistically viable fitting, the reported surface binding affinities are the average of the two, as seen in **Figure 10**. Error was propagated through the average.

4.2.3 The Stoichiometry of Complex Formation

As stated previously, all of the reported binding information assumes 1:1 Zn^{2+}–carboxylate complexation at the air-water interface. However, this may not be an electrostatically preferred system because the Zn^{2+} ion has a divalent positive charge while the carboxylate group has a monovalent negative charge, meaning that the 1:1 complex would carry a 1+ charge. A 1:2 Zn^{2+}–

carboxylate complex, however, would carry an overall charge of zero. One proposed mechanism for the formation of the 1:2 complex is a ternary single-step reaction in which the aqueous zinc ion and two free, adjacent carboxylate headgroups form bind together all at once (**Equation 4**).[55]

$$K_{a1}[Zn^{2+}][SA^{-}]^2 = [Zn(SA)_2] \quad (4)$$

$$A = A_{max}\frac{1+8K_{a1}[S][Zn^{2+}]-\sqrt{1+16K_{a1}[S][Zn^{2+}]}}{8K_{a1}[S][Zn^{2+}]} \quad (5)$$

The 1:2 complexation single-step adsorption model is given as **Equation 5**, where $K_{a1}[S]$ is the binding parameter of the single-step reaction and [S] specifically is the density of surface binding sites. When applied to the IRRAS data, this adsorption model provides a poor fit with low R^2 values. The poor fit may be due to the fact that ternary reactions are not kinetically favorable and are unlikely to occur spontaneously. Therefore, this ternary mechanism of binding will not be considered further.

Another proposed mechanism for the formation of the 1:2 Zn^{2+}–carboxylate complex is a two-step process. In the first step, which is bimolecular, a zinc ion binds to a single carboxylate headgroup to form a 1:1 Zn^{2+}–carboxylate complex (**Equation 6**). In the second step, an adjacent and free carboxylate headgroup binds to the existing complex to form a zinc ion bound by two carboxylate headgroups (**Equation 7**).[55]

Step 1: $$K_a[Zn^{2+}][SA^{-}] = [Zn(SA)]^{+} \quad (6)$$

Step 2: $$K_b[SA^{-}][Zn(SA)]^{+} = [Zn(SA)_2] \quad (7)$$

$$A = A_{max}\frac{1+8K_b[S]K_a[Zn^{2+}]-(K_a[Zn^{2+}])^2+(K_a[Zn^{2+}]-1)\cdot\sqrt{(K_a[Zn^{2+}]+1)^2+16K_b[S]K_a[Zn^{2+}]}}{16K_b[S]K_a[Zn^{2+}]} \quad (8)$$

The 1:2 complexation two-step adsorption model is given as **Equation 8**, where $K_b[S]$ is the binding parameter of Step 2 and [S] is the density of surface binding sites.[55] Step 1 is equal to the 1:1 binding mechanism assumed for the previously calculated Langmuir adsorption, and therefore K_a here is equal to the K_a found by Langmuir fitting.[55] Since K_a in the two-step equation is equal to the Langmuir binding constant, $K_b[S]$ is a parameter that is indicative of any 1:2 binding above and beyond the binding achieved in Step 1.[55] The two-step adsorption model fits the data much more reliably than the single-step model. For each ratio of SA:OD, the two-step adsorption curve consistently falls between the Langmuir curve and the Langmuir-Freundlich curve, with R^2 values in the same range. Values from the fit are given in **Figure 11**.

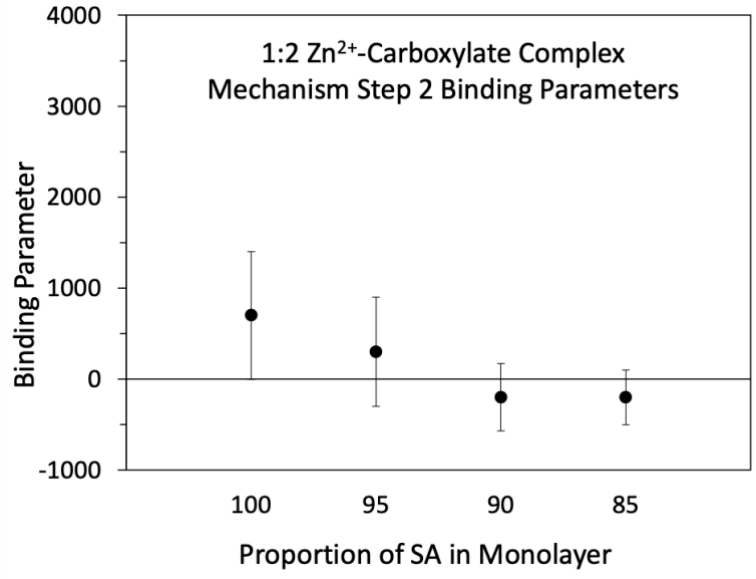

SA:OD Ratio	Binding Parameter
100:0	0.7 (0.7) × 10^3
95:5	0.3 (0.6) × 10^3
90:10	-0.2 (0.4) × 10^3
85:15	-0.2 (0.3) × 10^3

Figure 11. Summary of the binding parameters for Step 2 in the mechanism of 1:2 Zn^{2+}–carboxylate complex formation for each of the four reported monolayer compositions with standard error

The trend in binding parameters reveals that when there is a higher proportion of SA in the monolayer, 1:1 surface complexes are more likely to complete Step 2 of the mechanism to become

1:2 Zn^{2+}–carboxylate complexes. This trend is kinetically viable because as the SA monolayer is diluted with OD, there is a decreased probability that any given molecule adjacent to a 1:1 complex is SA. When there are less adjacent SA molecules available, it may be more energetically taxing for the 1:1 complex to bind another carboxylate headgroup. A schematic of this motif is presented in **Figure 12**. There is a distinct divide in binding parameter value between the upper two and the lower two SA:OD ratios: the upper two are positive, while the lower two are negative. This may indicate that at some point between the 95:5 and 90:10, the proportion of OD in the monolayer becomes too high to support significant 1:2 Zn^{2+}–carboxylate complex formation.

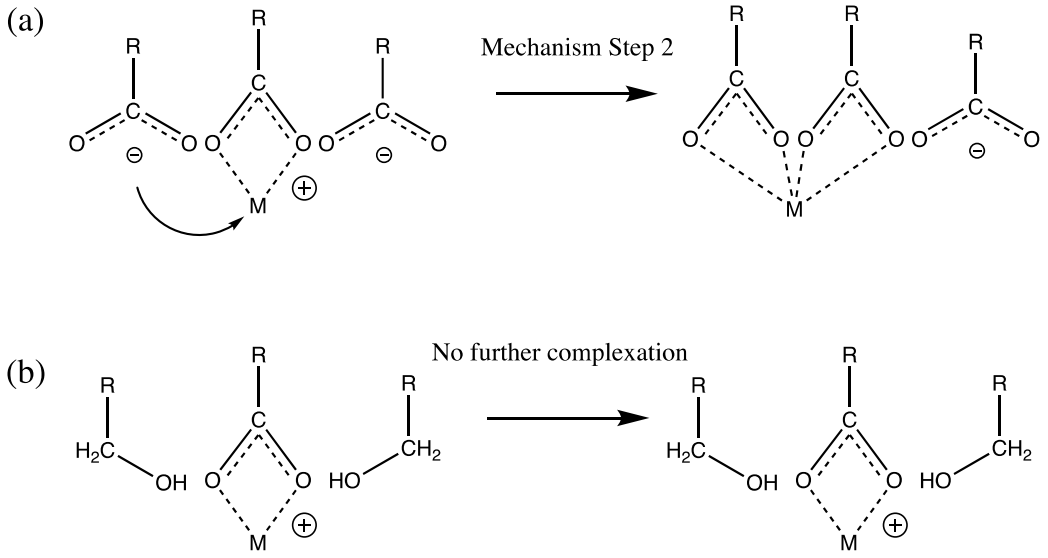

Figure 12. Proposed motif of mechanism Step 2 in the two-step formation of the 1:2 Zn^{2+}–carboxylate complex at the air-water interface. M represents divalent Zn^{2+}. (a) A monolayer environment rich in SA is conducive to successful completion of Step 2, but as the proportion of OD increases (b) the likelihood of Step 2 completion is diminished.

4.3 Trends and Comparisons in Surface Binding Strength

The 1:1 Zn^{2+}–carboxylate surface binding affinity values for SA:OD ratios of 100:0, 95:5, 90:10, and 85:15 were respectively found to be 3000, 2500, 1400, and 1800 M^{-1}. At the higher two

ratios, some of these complexes bind an additional carboxylate headgroup to form a 1:2 complex, but this is not observed in the lower two ratios. All binding constants were quantified based on monolayers with a surface pressure of 35 mN/m, an approximate mean molecular area of 21.5 $Å^2$/molecule, and in the highly ordered untilted condensed phase. For comparison in magnitude, trace metal surface binding affinities to a pure monolayer of 1,2-dipalmitoyl-sn-glycero-3-phosphate (DPPA) were quantified by Zhang et al. using methods similar to those reported here, but with surface tension data instead of spectral peak areas.[18] They also explored a higher, less ocean-relevant concentration regime of 0 to 95 mM for each metal. The reported surface binding affinities range from 27 to 90 with the exception of Zn^{2+} which was found to have an "abnormally high" value of 700.[18] These metal–phosphate surface binding affinities found by Zhang are considerably smaller than the Zn^{2+}–carboxylate surface binding affinities found here. This difference in magnitude may be attributed to the difference in technique and/or weaker ability of the phosphate headgroup to chelate metals when compared to the carboxylate headgroup.

Unfortunately, no previous studies have quantified metal–carboxylate surface binding affinities, so bulk values must be used for comparison. The zinc–acetate bulk binding affinity has been reported between 5.75 and 38.90 M^{-1} and the zinc–EDTA bulk binding affinity is 10^{16} M^{-1}.[56,57] It was expected for zinc–EDTA complexation to have a much higher binding affinity than those reported here due to the sheer strength of EDTA coordination, especially with zinc. EDTA is known to bind zinc so tightly that it can selectively deplete a solution of its zinc content, even if the solution contains other divalent metals.[57] Nevertheless, binding constants on the order of 10^3 M^{-1} are very large. The bulk carboxylate ligand comparison, zinc-acetate, binds about 300 times more weakly than the zinc-SA surface complex. The difference between surface and bulk binding is the chemical environment. These results, along with previous studies, are in agreement that the

surface environment enhances binding. Proposed reasons for surface binding enhancement include the surface environment having a reduced binding hydration penalty when compared to the bulk and the surface environment having a lower dielectric constant, which can lower the free energy of ion association to the monolayer.[41]

As the proportion of SA in the monolayer decreases, the Zn^{2+}–carboxylate surface binding affinity also decreases when analyzed between 100:0 and 90:0. However, the trend reverses as the ratio becomes 85:15. This may indicate a simple negative correlation between proportion of SA and binding affinity, or it could signify a more complex correlation with 90:10 as a local minimum. The observed negative correlation may be caused by OD interrupting the lateral, hexagonally packed interactions between SA molecules, thus pulling electron density away from the carboxylate groups and reducing their ability to chelate zinc. In the case that 90:10 is a local minimum, it would indicate that lateral disruptions caused by OD increasingly hinder the binding ability of SA down to the 90:10 ratio, and then reverse effects to promote stronger binding at lower ratios. This idea is particularly interesting because 90:10 was recently found to be the oceanic ratio of fatty acid to fatty alcohol.[16] If that ratio truly minimizes metal–carboxylate binding interactions, then binding is minimized in systems with oceanic conditions such as the SSML.

CHAPTER 5: CONCLUSIONS AND FUTURE WORK

Mixed monolayers, as opposed to pure monolayers, are more representative of real-world atmospheric and oceanic systems. However, the majority of laboratory monolayer experiments only consider a pure monolayer, especially in studies that consider metal surface binding. This knowledge gap is significant and may impact current understandings of important chemical and environmental processes such as transport of metal cations into the atmosphere. In this study, zinc–carboxylate surface binding was probed as a function of monolayer composition using Π-A isotherms and IRRAS. All systems were studied with a surface pressure of 35 mN/m, a mean molecular area of approximately 21.5 $Å^2$/molecule, and an untilted condensed monolayer structure. Binding affinities for 1:1 Zn^{2+}–carboxylate surface complexes were found for each of the four ratios of SA:OD studied (100:0, 95:5, 90:10, and 85:15) via Langmuir and Langmuir-Freundlich adsorption models. All 1:1 Zn^{2+}–carboxylate surface binding affinities were found to be on the order of 10^3, about 300 times stronger than the analogous bulk binding process, indicating enhanced binding at the interface. Monolayer composition was found to influence binding with an observable negative correlation between proportion of OD and Zn^{2+}–carboxylate surface binding. Finally, the potential of each system to form 1:2 Zn^{2+}–carboxylate surface complexes was analyzed using a bivalent binding model. It was found that the two highest monolayer ratios, 100:0 and 95:5, are able to support formation of 1:2 Zn^{2+}–carboxylate surface complexes via two-step reaction mechanism. Future work for this project includes repeating experiments under N_2 flow to minimize noise due to water vapor, thus increasing statistical confidence in observed trends. Additionally, studying different ratios of the SA:OD system or the adsorption of different metals to the current ratios would be beneficial in gaining a broader understanding of the impacts of monolayer

composition on metal–carboxylate surface binding. Such advances in the understanding of interfacial adsorption processes will help to improve the understanding of aerosol impacts on climate.

CHAPTER 6: REFERENCES

(1) Characteristic Features of Surfactants. In *Surfactants and Interfacial Phenomena*; John Wiley & Sons, Ltd, 2012; pp 1–38.

(2) Donaldson, D. J.; Vaida, V. The Influence of Organic Films at the Air−Aqueous Boundary on Atmospheric Processes. *Chem. Rev.* **2006**, *106* (4), 1445–1461.

(3) Cochran, R. E.; Jayarathne, T.; Stone, E. A.; Grassian, V. H. Selectivity Across the Interface: A Test of Surface Activity in the Composition of Organic-Enriched Aerosols from Bubble Bursting. *J. Phys. Chem. Lett.* **2016**, *7* (9), 1692–1696.

(4) Resch, F.; Afeti, G. Film Drop Distributions from Bubbles Bursting in Seawater. *J. Geophys. Res. Oceans* **1991**, *96* (C6), 10681–10688.

(5) Liepert, B. G. Observed Reductions of Surface Solar Radiation at Sites in the United States and Worldwide from 1961 to 1990. *Geophys. Res. Lett.* **2002**, *29* (10), 61-1-61–64.

(6) DeMott, P. J.; Hill, T. C. J.; McCluskey, C. S.; Prather, K. A.; Collins, D. B.; Sullivan, R. C.; Ruppel, M. J.; Mason, R. H.; Irish, V. E.; Lee, T.; Hwang, C. Y.; Rhee, T. S.; Snider, J. R.; McMeeking, G. R.; Dhaniyala, S.; Lewis, E. R.; Wentzell, J. J. B.; Abbatt, J.; Lee, C.; Sultana, C. M.; Ault, A. P.; Axson, J. L.; Diaz Martinez, M.; Venero, I.; Santos-Figueroa, G.; Stokes, M. D.; Deane, G. B.; Mayol-Bracero, O. L.; Grassian, V. H.; Bertram, T. H.; Bertram, A. K.; Moffett, B. F.; Franc, G. D. Sea Spray Aerosol as a Unique Source of Ice Nucleating Particles. *Proc. Natl. Acad. Sci. U. S. A.* **2016**, *113* (21), 5797–5803.

(7) Vaida, V. Atmospheric Radical Chemistry Revisited. *Science* **2016**, *353* (6300), 650–650.

(8) Cochran, R. E.; Laskina, O.; Jayarathne, T.; Laskin, A.; Laskin, J.; Lin, P.; Sultana, C.; Lee, C.; Moore, K. A.; Cappa, C. D.; Bertram, T. H.; Prather, K. A.; Grassian, V. H.;

Stone, E. A. Analysis of Organic Anionic Surfactants in Fine and Coarse Fractions of Freshly Emitted Sea Spray Aerosol. *Environ. Sci. Technol.* **2016**, *50* (5), 2477–2486.

(9) Langmuir Films. *Nanoscience Instruments*.

(10) Ellison, G. B.; Tuck, A. F.; Vaida, V. Atmospheric Processing of Organic Aerosols. *J. Geophys. Res. Atmospheres* **1999**, *104* (D9), 11633–11641.

(11) Rouvière, A.; Ammann, M. The Effect of Fatty Acid Surfactants on the Uptake of Ozone to Aqueous Halogenide Particles. *Atmospheric Chem. Phys.* **2010**, *10* (23), 11489–11500.

(12) Griffith, E. C.; Adams, E. M.; Allen, H. C.; Vaida, V. Hydrophobic Collapse of a Stearic Acid Film by Adsorbed L-Phenylalanine at the Air–Water Interface. *J. Phys. Chem. B* **2012**, *116* (27), 7849–7857.

(13) Cheng, S.; Li, S.; Tsona, N. T.; George, C.; Du, L. Insights into the Headgroup and Chain Length Dependence of Surface Characteristics of Organic-Coated Sea Spray Aerosols. *ACS Earth Space Chem.* **2019**, *3* (4), 571–580.

(14) Li, S.; Du, L.; Wei, Z.; Wang, W. Aqueous-Phase Aerosols on the Air-Water Interface: Response of Fatty Acid Langmuir Monolayers to Atmospheric Inorganic Ions. *Sci. Total Environ.* **2017**, *580*, 1155–1161.

(15) Ochshorn, E.; Cantrell, W. Towards Understanding Ice Nucleation by Long Chain Alcohols. *J. Chem. Phys.* **2006**, *124* (5), 054714.

(16) Perkins, R. J.; Vazquez de Vasquez, M. G.; Beasley, E. E.; Hill, T. C. J.; Stone, E. A.; Allen, H. C.; DeMott, P. J. Relating Structure and Ice Nucleation of Mixed Surfactant Systems Relevant to Sea Spray Aerosol. *J. Phys. Chem. A* **2020**, *124* (42), 8806–8821.

(17) Adams, E. M.; Verreault, D.; Jayarathne, T.; Cochran, R. E.; Stone, E. A.; Allen, H. C. Surface Organization of a DPPC Monolayer on Concentrated $SrCl_2$ and $ZnCl_2$ Solutions. *Phys. Chem. Chem. Phys.* **2016**, *18* (47), 32345–32357.

(18) Zhang, T.; Fiamingo, M.; Allen, H. C. Trace Metal Enrichment Driven by Phosphate Functional Group Binding Selectivity. *J. Geophys. Res. Oceans* **2018**, *123* (8), 5286–5297.

(19) Li, S.; Du, L.; Tsona, N. T.; Wang, W. The Interaction of Trace Heavy Metal with Lipid Monolayer in the Sea Surface Microlayer. *Chemosphere* **2018**, *196*, 323–330.

(20) Simon-Kutscher, J.; Gericke, A.; Hühnerfuss, H. Effect of Bivalent Ba, Cu, Ni, and Zn Cations on the Structure of Octadecanoic Acid Monolayers at the Air−Water Interface As Determined by External Infrared Reflection−Absorption Spectroscopy. *Langmuir* **1996**, *12* (4), 1027–1034.

(21) Kumar, N.; Wang, L.; Siretanu, I.; Duits, M.; Mugele, F. Salt Dependent Stability of Stearic Acid Langmuir–Blodgett Films Exposed to Aqueous Electrolytes. *Langmuir* **2013**, *29* (17), 5150–5159.

(22) Straub, D. J.; Lee, T.; Collett, J. L. Chemical Composition of Marine Stratocumulus Clouds over the Eastern Pacific Ocean. *J. Geophys. Res. Atmospheres* **2007**, *112* (D4).

(23) Barker, D. R.; Zeitlin, H. Metal-Ion Concentrations in Sea-Surface Microlayer and Size-Separated Atmospheric Aerosol Samples in Hawaii. *J. Geophys. Res. 1896-1977* **1972**, *77* (27), 5076–5086.

(24) Bruland, K. W.; Lohan, M. C. 6.02 Controls of Trace Metals in Seawater. 25.

(25) Adams, E. M.; Wellen, B. A.; Thiraux, R.; Reddy, S. K.; Vidalis, A. S.; Paesani, F.; Allen, H. C. Sodium–Carboxylate Contact Ion Pair Formation Induces Stabilization of Palmitic Acid Monolayers at High PH. *Phys. Chem. Chem. Phys.* **2017**, *19* (16), 10481–10490.

(26) Zhang, Z.; Liu, L.; Liu, C.; Cai, W. Studies on the Sea Surface Microlayer: II. The Layer of Sudden Change of Physical and Chemical Properties. *J. Colloid Interface Sci.* **2003**, *264* (1), 148–159.

(27) Ebling, A. M.; Landing, W. M. Sampling and Analysis of the Sea Surface Microlayer for Dissolved and Particulate Trace Elements. *Mar. Chem.* **2015**, *177*, 134–142.

(28) Chattoraj, D. K.; Birdi, K. S. Spread Monolayer. In *Adsorption and the Gibbs Surface Excess*; Chattoraj, D. K., Birdi, K. S., Eds.; Springer US: Boston, MA, 1984; pp 179–232.

(29) Li, S.; Du, L.; Zhang, Q.; Wang, W. Stabilizing Mixed Fatty Acid and Phthalate Ester Monolayer on Artificial Seawater. *Environ. Pollut. Barking Essex 1987* **2018**, *242* (Pt A), 626–633.

(30) Kartashynska, E. S.; Vysotsky, Y. B.; Vollhardt, D.; Fainerman, V. B.; Zakharov, A. Yu. Theoretical Description of Mixed Film Formation at the Air/Water Interface: Carboxylic Acids–Alcohols. *ACS Omega* **2018**, *3* (12), 16693–16705.

(31) Panda, A. K.; Nag, K.; Harbottle, R. R.; Possmayer, F.; Petersen, N. O. Thermodynamic Studies on Mixed Molecular Langmuir Films: Part 2. Mutual Mixing of DPPC and Bovine Lung Surfactant Extract with Long-Chain Fatty Acids. *Colloids Surf. Physicochem. Eng. Asp.* **2004**, *247* (1), 9–17.

(32) Seoane, R.; Miñones, J.; Conde, O.; Miñones, J.; Casas, M.; Iribarnegaray, E. Thermodynamic and Brewster Angle Microscopy Studies of Fatty Acid/Cholesterol Mixtures at the Air/Water Interface. *J. Phys. Chem. B* **2000**, *104* (32), 7735–7744.

(33) Lee, Y.-L.; Yang, Y.-C.; Shen, Y.-J. Monolayer Characteristics of Mixed Octadecylamine and Stearic Acid at the Air/Water Interface. *J. Phys. Chem. B* **2005**, *109* (10), 4662–4667.

(34) Ge, A.; Wu, H.; Darwish, T. A.; James, M.; Osawa, M.; Ye, S. Structure and Lateral Interaction in Mixed Monolayers of Dioctadecyldimethylammonium Chloride (DOAC) and Stearyl Alcohol. *Langmuir* **2013**, *29* (18), 5407–5417.

(35) Denton, J. K.; Kelleher, P. J.; Johnson, M. A.; Baer, M. D.; Kathmann, S. M.; Mundy, C. J.; Rudd, B. A. W.; Allen, H. C.; Choi, T. H.; Jordan, K. D. Molecular-Level Origin of the Carboxylate Head Group Response to Divalent Metal Ion Complexation at the Air–Water Interface. *Proc. Natl. Acad. Sci.* **2019**, *116* (30), 14874–14880.

(36) Wang, Y.; Du, X.; Guo, L.; Liu, H. Chain Orientation and Headgroup Structure in Langmuir Monolayers of Stearic Acid and Metal Stearate (Ag, Co, Zn, and Pb) Studied by Infrared Reflection-Absorption Spectroscopy. *J. Chem. Phys.* **2006**, *124* (13), 134706.

(37) Wellen, B. A.; Lach, E. A.; Allen, H. C. Surface PKa of Octanoic, Nonanoic, and Decanoic Fatty Acids at the Air–Water Interface: Applications to Atmospheric Aerosol Chemistry. *Phys. Chem. Chem. Phys.* **2017**, *19* (39), 26551–26558.

(38) Sutton, C. C. R.; da Silva, G.; Franks, G. V. Modeling the IR Spectra of Aqueous Metal Carboxylate Complexes: Correlation between Bonding Geometry and Stretching Mode Wavenumber Shifts. *Chem. – Eur. J.* **2015**, *21* (18), 6801–6805.

(39) Giner-Casares, J. J.; Brezesinski, G.; Möhwald, H. Langmuir Monolayers as Unique Physical Models. *Curr. Opin. Colloid Interface Sci.* **2014**, *19* (3), 176–182.

(40) Kaganer, V. M.; Möhwald, H.; Dutta, P. Structure and Phase Transitions in Langmuir Monolayers. *Rev. Mod. Phys.* **1999**, *71* (3), 779–819.

(41) Neal, J. F.; Zhao, W.; Grooms, A. J.; Flood, A. H.; Allen, H. C. Arginine–Phosphate Recognition Enhanced in Phospholipid Monolayers at Aqueous Interfaces. *J. Phys. Chem. C.* **2018**, *122* (46), 26362–26371.

(42) Mendelsohn, R.; Brauner, J. W.; Gericke, A. External Infrared Reflection Absorption Spectrometry of Monolayer Films at the Air-Water Interface. *Annu. Rev. Phys. Chem.* **1995**, *46* (1), 305–334.

(43) Blume, A.; Kerth, A. Peptide and Protein Binding to Lipid Monolayers Studied by FT-IRRA Spectroscopy. *Biochim. Biophys. Acta BBA - Biomembr.* **2013**, *1828* (10), 2294–2305.

(44) Attenuated Total Reflection Fourier Transform Infrared Microspectroscopy: Theory and Application to Polymer Samples. *Vib. Spectrosc.* **1996**, *11* (1), 29–36.

(45) Gaines, G. L. *Insoluble Monolayers at Liquid-Gas Interfaces*; Interscience Publishers: New York, **1966**.

(46) Cameron, D. G.; Casal, H. L.; Gudgin, E. F.; Mantsch, H. H. The Gel Phase of Dipalmitoyl Phosphatidylcholine. An Infrared Characterization of the Acyl Chain Packing. *Biochim. Biophys. Acta BBA - Biomembr.* **1980**, *596* (3), 463–467.

(47) Pfrang, C.; Rastogi, K.; Cabrera-Martinez, E. R.; Seddon, A. M.; Dicko, C.; Labrador, A.; Plivelic, T. S.; Cowieson, N.; Squires, A. M. Complex Three-Dimensional Self-Assembly in Proxies for Atmospheric Aerosols. *Nat. Commun.* **2017**, *8*.

(48) Rudd, B. A. W.; Vidalis, A. S.; Allen, H. C. Thermodynamic versus Non-Equilibrium Stability of Palmitic Acid Monolayers in Calcium-Enriched Sea Spray Aerosol Proxy Systems. *Phys. Chem. Chem. Phys.* **2018**, *20* (24), 16320–16332.

(49) Schaefer, C. E.; Culina, V.; Nguyen, D.; Field, J. Uptake of Poly- and Perfluoroalkyl Substances at the Air–Water Interface. *Environ. Sci. Technol.* **2019**, *53* (21), 12442–12448.

(50) Khayyun, T. S.; Mseer, A. H. Comparison of the Experimental Results with the Langmuir and Freundlich Models for Copper Removal on Limestone Adsorbent. *Appl. Water Sci.* **2019**, *9* (8), 170.

(51) Soares, J. C.; Soares, A. C.; Pereira, P. A. R.; Rodrigues, V. da C.; Shimizu, F. M.; Melendez, M. E.; Neto, C. S.; Carvalho, A. L.; Leite, F. L.; Machado, S. A. S.; Oliveira, O. N. Adsorption According to the Langmuir–Freundlich Model Is the Detection Mechanism of the Antigen P53 for Early Diagnosis of Cancer. *Phys. Chem. Chem. Phys.* **2016**, *18* (12), 8412–8418.

(52) Langmuir, I. THE ADSORPTION OF GASES ON PLANE SURFACES OF GLASS, MICA AND PLATINUM. *J. Am. Chem. Soc.* **1918**, *40* (9), 1361–1403.

(53) Henry, D. C. LX. *A Kinetic Theory of Adsorption*. *Lond. Edinb. Dublin Philos. Mag. J. Sci.* **1922**, *44* (262), 689–705.

(54) Jeppu, G. P.; Clement, T. P. A Modified Langmuir-Freundlich Isotherm Model for Simulating PH-Dependent Adsorption Effects. *J. Contam. Hydrol.* **2012**, *129–130*, 46–53.

(55) Binding of a Monoclonal Antibody and Its Fab Fragment to Supported Phospholipid Monolayers Measured by Total Internal Reflection Fluorescence Microscopy. *Biophys. J.* **1990**, *58* (5), 1235–1249.

(56) Bunting, J. W.; Thong, K. M. Stability Constants for Some 1:1 Metal–Carboxylate Complexes. *Can. J. Chem.* **1970**, *48* (11), 1654–1656.

(57) Nyborg, J. K.; Peersen, O. B. That Zincing Feeling: The Effects of EDTA on the Behaviour of Zinc-Binding Transcriptional Regulators. *Biochem. J.* **2004**, *381* (Pt 3).